Journal of King Saud University - Science 36 (2024) 103160

HOSTED BY

Contents lists available at ScienceDirect

Journal of King Saud University - Science

journal homepage: www.sciencedirect.com

Full Length Article

Evaluation of the capability of coumarin dye as a liquid scintillator for gamma ray detection and compton edge localization

Saradh Prasad [a,b], Nassar N. Asemi [a,b], Saad Aldawood [b], Mohamad S. AlSalhi [a,b,*]

[a] Research Chair on Laser Diagnosis of Cancers, Department of Physics and Astronomy, College of Science, King Saud University, P.O. Box: 2455, Riyadh 11451, Saudi Arabia

[b] Department of Physics and Astronomy, College of Science, King Saud University, P.O. Box: 2455, Riyadh 11451, Saudi Arabia

ARTICLE INFO

Keywords:
Liquid scintillator
Gamma detection
Light yield
Coumarin dye
Compton edge
GEANT4 simulation

ABSTRACT

In this work, we developed a highly sensitive liquid scintillator (LS) using Coumarin 450 (C450) dye to detect gamma ray and localize Compton edges (CEs). C450 exhibited absorption and fluorescence peaks at 350 nm and 407 nm, respectively, in toluene, at an optimized concentration (3 mM). The LS, contained in a standard glass container (1.8 cm diameter, 3.6 cm height), showed an emission peak in the blue region, matching the high quantum yield of typical PMT photocathodes. We exposed the LS to various gamma radiation sources (^{137}Cs, ^{60}Co, and ^{22}Na), recording responses for different PMT voltages. Gaussian fitting of pulse height distribution spectrum allowed CE identification at the half-height for all PMT voltages. We compared theoretical and experimental results to a GEANT4-simulated detector, obtaining CE positions for radiation interactions and scintillation photon transport. The calibrated GEANT4 simulation was compared to experimental spectra to locate the Compton edges.

1. Introduction

The spread of nuclear energy is inevitable due to advances in safety standards and the compact designs of nuclear reactors. It is possible that nuclear energy will power neighborhoods in the near future. Therefore, the need for new low-cost radiation detectors is increasing. Similarly, high-energy particle accelerators require detection systems that can respond faster to particle collision events.

Liquid scintillators are used to detect neutrons, gamma ray, neutron-gamma discrimination, and time-of-flight research due to their superior pulse height and timing characteristics (Gul et al., n.d.; Knoll, 2010; Naqvi et al., 1991). The basic principle is that high energy radiation interacts with LS molecules to produce photons of energy range that is detectable by a photoreactors such as PMT. LSs are straightforward to erect, maintain and refurbish from the operational point of view. Currently, 2,5-Diphenyloxazole (PPO) (Asemi et al., 2022; Zaitseva et al., n.d.), linear alkyl benzene (LAB) (Li et al., 2016), 1,4-bis(2-methylstyryl)benzene (PARK et al., 2009), 1,4-bis(5-phenyloxazol-2-yl)benzene (POPOP) (Aldawood et al., n.d.; Zhao et al., 2021) have been used as LS in high energy radiation/particle detection spectroscopy due to their high flash point, good light yield, and is compatible with photomultiplier tubes (PMTs). Despite the availability of various commercial and experimental LS, they are not extensively used due to it high price.

On the other hand, due to their excellent optical properties are considered to advantages, such as a high extinction coefficient, significant Stokes' shift (Mannekutla et al., n.d.), light emission devices (Inagaki et al., 2009), and quantum yield (Zhang and Li, 2013) coumarin dyes emitting in blue–green regions (400–550 nm) have been used as fluorescent dye probes, optical brighteners, fluorescent indicators, and solar energy collectors (Arora et al., 1982; Jones et al., 1985; Mahadevan et al., n.d.; Mohan et al., n.d.). Many coumarin dyes have shown improved optical and solubility properties due to substitution moieties and intramolecular charge transfer (ICT)(Matta et al., 2017), and Förster resonance energy transfer (FRET) is a donor (Porel et al., 2012) or acceptor (Brites et al., n.d.) due to coumarin's sizeable dipole–dipole moment [15]. The most critical application of coumarin dyes is its use in lasers that produce light at different wavelengths in the visible region (Ibnaouf et al., 2012; Prasad et al., 2022, 2020). The substitution moieties improve the solidarity in various solvents and thus increase the emission quantum yield (Ibnaouf et al., 2012), and they exhibit solvatochromic behavior (Ravi et al., n.d.). However, the currently investigated C450 may have limitations such as limited energy resolution, relatively low light yield, calibration errors due to photo-degradation,

* Corresponding author.
E-mail addresses: srajendra@ksu.edu.sa (S. Prasad), nasemi@ksu.edu.sa (N.N. Asemi), sdawood@ksu.edu (S. Aldawood), malsalhi@ksu.edu.sa (M.S. AlSalhi).

https://doi.org/10.1016/j.jksus.2024.103160
Received 11 October 2023; Received in revised form 27 February 2024; Accepted 8 March 2024
Available online 11 March 2024

and limited solubility in desired solvents (Gupta et al., 2012; Saxena et al., 2018).

Researchers have tried to evaluate coumarin dyes as LSs due to their desired features, such as high emission in the blue region, solubility in preferred solvents, and fast fluorescence. Previously, 7-diethylamino-4-methylcoumarin (MDAC) was used as a secondary dye, and 2,5-diphenyloxazole (PPO) was used as a primary dye (Zaitseva et al., n.d.) in a plastic scintillator. It has shown good pulse shape discrimination (PSD) in neutron detection (Zaitseva et al., 2020). Coumarin 6 and 1,1-di-(*tert*-butylperoxy)-3,3,5-trimethylcyclohexane were used as wavelength shifters in plastic scintillator designed by T. J. Hajagos et al. (Hajagos et al., 2016). Various commercially available coumarin dyes were embedded in a polystyrene matrix and tested for plastic scintillation to detect gamma ray, as reported by A. Pla-Dalmau (Pla-Dalmau et al., 1996). In a different approach, Feroz A. Mir used naturally occurring coumarins such as osthol [7-methoxy-8-(3-methylbut-2-enyl) coumarin] (Mir et al., 2014) and 7-hydroxy-8-*O*-β-glycosylbenzopyranone (Mir et al., 2016) extracted from plants and evaluated the effects of gamma radiation on their optical properties. In our recent work, we have investigated a coumarin dye (DAMC) for its ability to detect gamma ray and it produced reasonable signal in response to gamma radiation (Aldawood et al., n.d.).

Even though there have been studies reported in the past that have utilized coumarin in gamma radiation, they either use it as a primary dye or as a wavelength shifter. Only a few reports have investigated the effects of gamma-ray radiation to change in optical properties of coumarin, like a dosimeter and not as a scintillator. In this context, we investigated pure C450 in liquid media (toluene) as a liquid scintillator (LS). This could be the first study of pure coumarin C450 as a LS, which has the advantages of low opaqueness and self-absorption compared to multi-dye cocktail based LSs. In addition, we compared the experimental light yield output and the CE localization of these LSs with the GEANT4 simulation results.

2. Materials and methods

2.1. Materials

The molecular structure of C450 is shown in Fig. 1 and it has a molecular weight of 217 g/mol. According to the information provided by the supplier, C450 powder has a purity level of 98 %. Toluene is sourced from Luba Chemicals Ltd.

2.2. Optical studies

A Perkin Elmer spectrophotometer (Lambda 950) and a spectrofluorometer (LS-55) were used to measure the absorption and emission spectra of the samples over the wavelength ranges of 300 to 1000 and 300 to 800 nm, respectively.

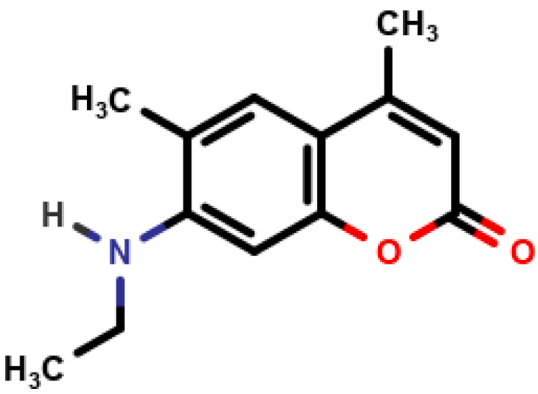

Fig. 1. molecular structure of the C450 dye.

2.3. Sample preparations

For experimentation, we prepared three cylindrical liquid cells of dimensions given in Supplementary Fig. S1. The cells all have a diameter of 1 in, a height of 0.5 in and a volume of 5 ml. Liquid scintillator 1 (LS1) contains 4.8 mg of C450 dissolved in 5 ml of toluene (0.11 wt%). The mixture was heated to 80 °C and then sonicated for 10 min, this removes any possible of aggregation of C450. In LS2, the weight of C450 was doubled to 0.22 wt% by dissolving 9.3 mg of C450 in 5 ml toluene. LS3 contains 14.4 mg of C450 dissolved in 5 ml toluene (0.33 wt%). Note that the labeling of LS1, 2 and 3 represents the liquid scintillator depending on the coumarin concentration. Fig. 2 shows LS1 (a) in ambient light and (b) exposed to UV light.

2.4. Scintillation experiments

The gamma source was Cs-137, Co-60, and Na-22, and the detector was a PMT (Hamamatsu R6094 with Bialkali photocathodes) connected to a multichannel analyzer (MCA) [manufacturer: CAEN, Model: N975 contains an 13 bit analog to digital converter (ADC) with 8192 channels, 0.8 μs conversion time]. The main MCA converts the analog pulses to digital pulses, assigns each signal to an appropriate energy channel based on its amplitude, sorts them according to height, and then counts the number in each channel (window) to give a spectral (energy) distribution of the fast electrons (Tsoulfanidis and Landsberger, 2021). The details of the experimental setup have been explained in our previous study (Asemi et al., 2022). The voltage of PMT varied from −865 V to −985 V to study the response of LS1, LS2 and LS3. This range is selected due to highest quantum yield of PMT tube is optimal in this range according to the data sheet and voltage is varies in steps of 20 V. However, in order to concise the discussion and results we compared different LSs in terms of counts and CE estimation at a PMT −925 V. to avoid background noise we increased the threshold voltage of MCA to 150 mV using control software, this makes the background noise negligible.

2.5. Determination of compton edge

The following equation can be used to determine the theoretical Compton edge's value (Knox et al., n.d.; Tsoulfanidis and Landsberger, 2021):

$$E_{CE} = \frac{2E_\gamma^2}{m_e c^2 + 2E_\gamma} \tag{1}$$

where E_{CE} is the CE electron kinetic occurring in 180° scattering, m_e is the electron mass, c is the speed of light, and E_γ represents the energy of the incident photon.

Assuming that the Compton edge is not easily discernible, the shoulder and tail portion of the pulse height distribution can be expressed in terms of a Gaussian distribution in the form (Chikkur and Umakantha, 1973):

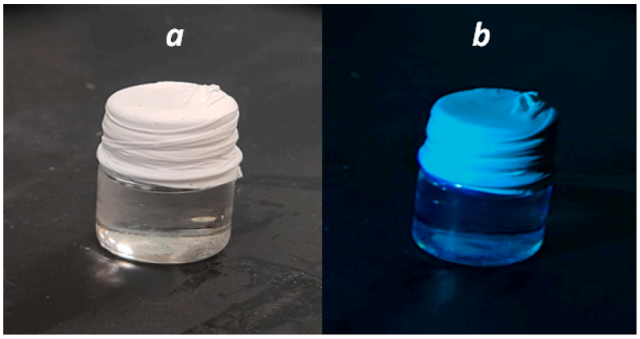

Fig. 2. LS1 (a) in ambient light (b) exposed to UV light.

$$C(n) = \frac{1}{\sigma\sqrt{(2\pi)}}\exp\left[-(N-\bar{N})^2/2\sigma^2\right] \quad (2)$$

where N is the energy, $\bar{N}$ is the mean value and σ is the standard deviation, where $N > \bar{N}$. Thus, the following equation can be regarded as the pulse height corresponding to the channel number of the CE:

$$N_C = \bar{N} + \sqrt{2\ln(2\sigma)} \quad (3)$$

2.6. GEANT4 simulation configuration

The simulated LS is a cylindrical scintillator with dimensions of 3 × 2 cm enclosed by a 1 mm thick Teflon tape on its front and side faces. A point source of Cs-137, Co-60 and Na-22 were used in simulation with a distance 5 cm from the LS. The bottom side of the LS is coupled to a PMT. The front face of the PMT is a cylindrical glass plate coupled with optical grease. The PMT is designed as a 2 cm diameter glass tube. The simulation was performed using the decay time of 4.85 ns for C450 reported previously (Dhenadhayalan et al., 2021). Note that for most coumarin-based dyes, the fluorescence decay time is approximately 4–5 ns (Das and Sarkar, 2012). Hence, we fed the simulator with 4.85 ns for both fast and slow decay components. The simulated energy spectra were calculated using collected photon counts at the PMT surface. We know that the LS photons originate from secondary electrons produced by gamma interactions with the LS. Fig. 3 provides a visual representation of the schematic diagram for the GEANT4 simulation code. The simulated LS is then tracked by a point gamma source that is placed in front of the LS connected to the PMT. The number of scintillation photons produced in the event (simulated for a defined time of exposure) is registered, and then the corresponding optical photons reach the PMT.

3. Results and discussion

3.1. Optical properties

Normalized absorption and photoluminescence (PL) spectra of coumarin at a concentration of 3 mol/m^3 in toluene are displayed in Fig. 4. The absorption spectrum of C450 showed a peak at 349 nm and a shoulder at 363 nm. In PL, a peak at 407 nm was observed, which can be attributed to the $S_{0\text{-}0}$ transition. The stokes' shift was measured to 58 nm, with minimal overlap between absorption and PL. The absorption spectrum was measure at 3 mM concentration in toluene because above which the spectrum was saturated, which would violate the Beer – Lambrate law for optical parameter calculations. And the PL of same concentration is measure and normalized to compare the stokes' shift and spectral overlap.

The normalized PL spectra of LS with different concentrations of C450 in toluene are shown in Fig. 5. The excitation wavelength was 349 nm (absorption peak). The same concentration were solutions utilized to fabricated LSs. The emission spectra exhibited an increased redshift for higher concentrations. The maximum peak intensity for LS1 is observed at 410 nm, while it is observed at 413 nm for LS2. On the other hand, the peak for LS3 was observed at approximately 420 nm. This effect could be attributed to the reabsorption process at a higher concentration of C450. However, the high concentration becomes essential for LS as it is inherently a low Z (mass) value media.

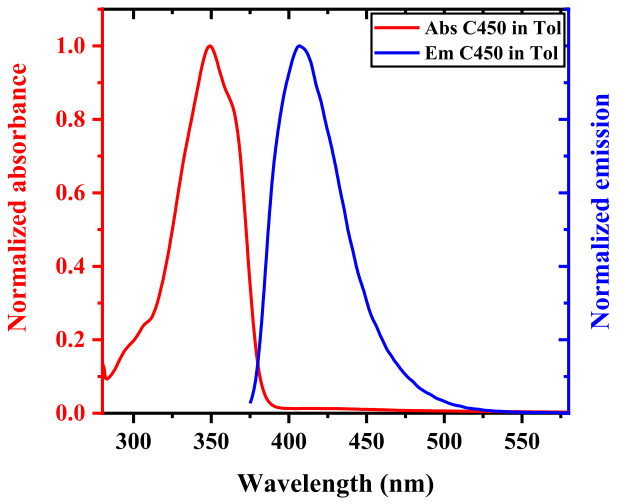

Fig. 4. Normalized absorption (red line) and emission (blue) of C450 in toluene at a concentration of 3 mol/m^3. (For interpretation of the references to colour in this figure legend, the reader is referred to the web version of this article.)

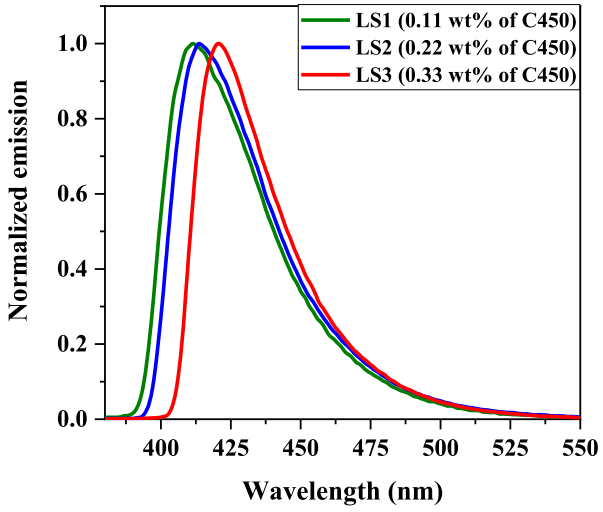

Fig. 5. Normalized emission spectra of fabricated liquid cells LS1, LS2, and LS3 for different concentrations of C450.

3.2. Gamma spectroscopy and localization of the Compton edge

The pulse height distribution of the Cs-137 gamma source of LS2 was determined at a PMT voltage of 925 V. Gaussian fitting of the shoulder and tail spectrum was used to determine the position of the Compton edge in LS2 and is illustrated in Fig. 6. The CE of LS2 is determined using

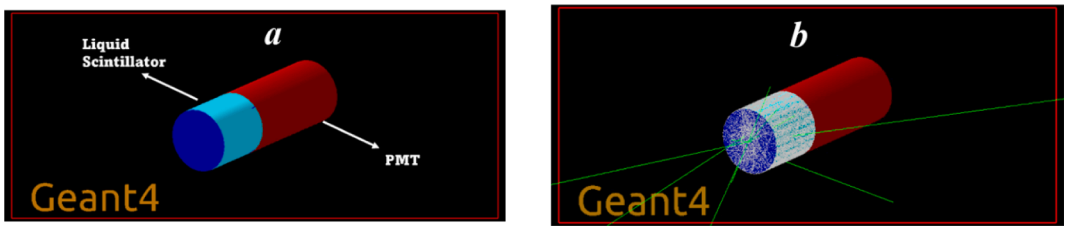

Fig. 3. GEANT4 visualization of a liquid scintillator based on C450 (a) before and (b) after events running.

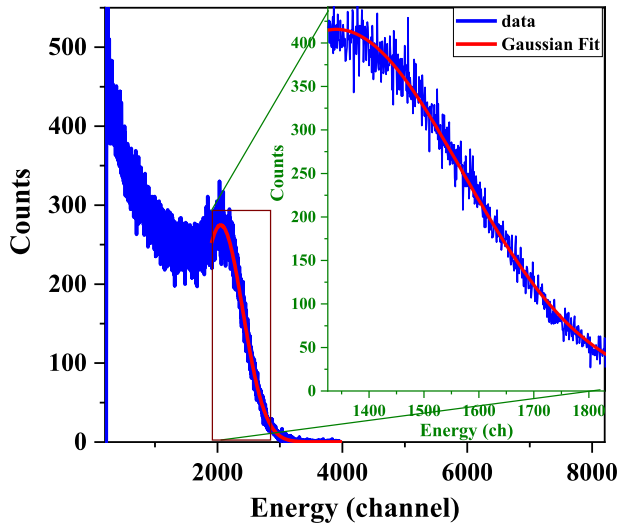

Fig. 6. Gaussian fit for the 662 keV gamma-ray Compton edge of the Cs-137 source using LS2.

Equation (3) (Chikkur and Umakantha, 1973), and it is explained in detail below.

The calculations were performed for other LSs (LS1 and LS3); for all LSs. Fig. 7 shows the pulse height of the Cs-137 gamma source for the fabricated liquid cells LS1, LS2, and LS3. The gamma ray photopeak CE of Cs-137 at 662 keV appeared at 3516 Ch for LS1, 2995 Ch for LS2, and 2755 Ch for LS3. Note the CE appears at half of the gaussian fitting. In cases of LSs with lower concentrations than LS1, the count rate was negligible, and further, the CE could not be distinguished from the background. The LS with the lowest concentration of C450 showed a higher CE channel sensitivity, and the CE was reduced by increasing the concentration of C450. However, the count rate of LS2 is higher than those of LS1 and LS3. Hence, the LS2 and LS3 CEs were 14.8 % and 21.6 % less than LS1, respectively. This indicates that the concentration to achieve a higher count rate and CE lies between these LS2 and LS3 of C450. On the other hand, for higher concentrations (LS3 and above), the LSs have lower CE than LS2. The lower detection efficiency of LS1, despite its higher channel sensitivity, could be influenced by factors such as self-absorption, re-emission and beyond. A plausible explanation could be that the quantum efficiency of the C450 dye at these low concentrations. While the higher channel sensitivity indicates efficient detection of photons that are produced, the lower concentration in LS1 might result in fewer scintillation events, leading to a reduced number of photons generated overall. The self-absorption coumarin dye at higher concentration was observed by Das et. al. in similar coumarin (C153) (Das and Sarkar, 2012).

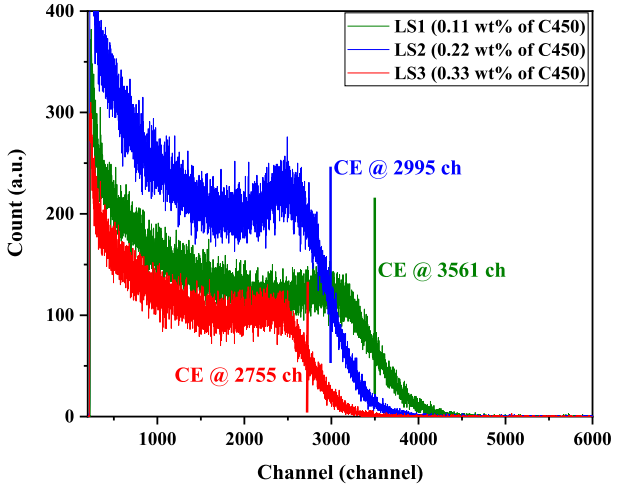

Fig. 7. Pulse height of the Cs-137 gamma source for the fabricated liquid cells LS1, LS2, and LS3.

Table. S1 shows the count rate observed by the three LSs for 20 min using a Cs-137 gamma source. We estimated the count rate by dividing the total counts by 20 min, and we calculated the uncertainty by dividing the square root of the total gross counts by the total time. The count rate achieved with LS2 was the highest among them. LS2 has a count rate per minute (CRM) of 34006, which was 140 % higher than the CRM of LS1 (24,266) and 218 % higher than the CRM of LS3 (15574).

The pulse height distribution details of the Cs-137 gamma source for different voltages are shown in Fig. 8. Table S2 shows the calculated values of Gaussian fitting (Compton peak) and the CE localization using LS1, LS2, and LS3 for different voltages. The trends in the data in Table S2 are illustrated in Fig. S2. The CE increased for all three LSs; LS1 showed the best CE of 5106 at 965 V among all LSs at all voltages used for testing. The NCE to the maximum height ratio (ρ) was approximately 0.5 ± 0.01 for all LSs. Similarly, the curve goodness of fit (χ^2) was more than 0.96 for all LSs at all voltages, except for LS2 at 965 V, which showed a χ^2 of 0.92.

In order to understand the response of LSs in terms of the pulse height distribution with respect to different bias voltage of PMT tube. To obtain the count/keV conversion factor for the energy calibration scale, we fit a linear relationship between the measured channel energies and theoretical CE energies for Cs-137, Na-22, and Co-60 gamma sources. Our previous study has more information about how the channels and energies have been calibrated (Asemi et al., 2022). The calibrated CE energies were compared to theoretical gamma-ray energy values calculated using Equation (1). The energy-calibrated spectra of LS1 are displayed in Fig. 9**.** The CE of LS1 corresponds to 328 keV for Cs-137 (511 keV) gamma energy, which is 3.5 % lower than the theoretical CE value of 340 keV. A CE of 494 keV was achieved for a gamma energy source of Na-22 (662 keV), which is 3.4 % greater than the theoretical value. There are two energies in the spectrum of the Co-60 gamma source, with CEs of 963.39 and 1118.11 keV, respectively, with an average value of 1040.75 keV. The experimental CE of Co-60 was 1039.50 keV, the error was only 0.12 %.

3.3. GEANT4 simulation results

As shown in Fig. 10, there are notable differences that discriminate CE between the experimental and simulation spectra. However, after calculation of CE from Gaussian fitting, the CE of experimental and simulated LS had an error (difference) of less than 5 %. In the case of Cs-137 (Fig. 10.a), the fitted experimental CE was 328 keV, which is 3.5 % lower than the theoretical value of 340 keV. The GEANT4 simulation of the same CE energy dropped to 471 keV, which is 1.3 % offset from the theoretical value.

The simulated Co-60 spectrum (Fig. 10b) exhibits two CEs, which correspond to 956 keV and 1113 keV, with differences of 0.8 % and 0.4 % from the calculated value, respectively. This average of 1034.5 keV, when compared to the experimental CE of 1039.5 keV, has a difference of 0.48 %. For Na-22 (Fig. 10.c), the simulated low energy CE at 334 keV had a difference of 1.8 % from the value calculated using Equation (1), and the high energy CE was at 1052 keV, which is almost identical to the calculated value using Equation (1). The experimental study was limited to the low energy of Na-22 due to the low resolution for higher energy. For this, the lower energy is fitted at 494 keV, which is 3.5 % lower than the theoretical value of 340 keV.

The accuracy of the simulation results was determined using the sharp parts and ignoring the incoherence near the end of the CE of each GEANT4 spectra. The inconsistency could be attributed to the low Z

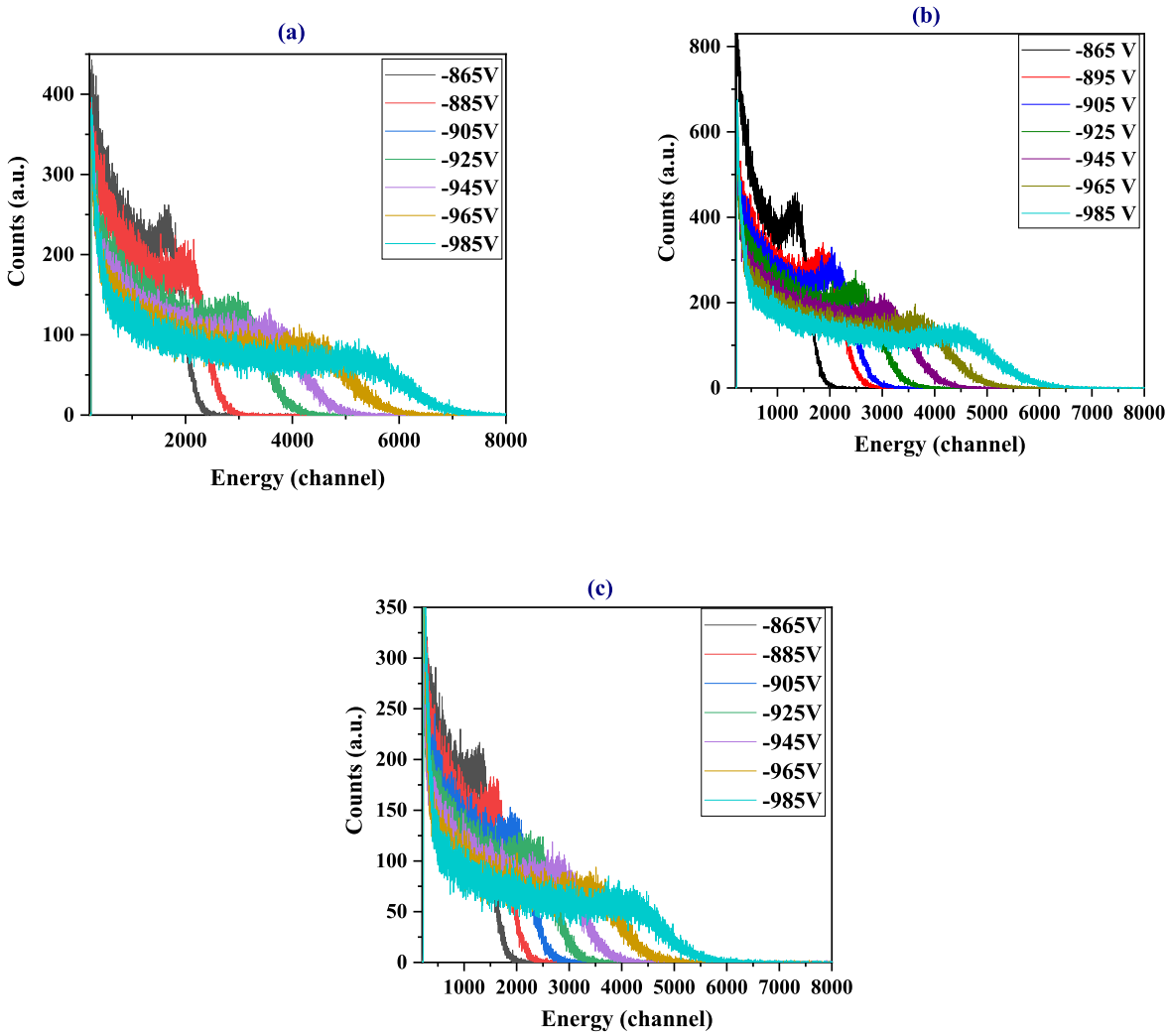

Fig. 8. Pulse height distribution of the Cs-137 gamma source at different voltages for (a) LS1, (b) LS2, and (c) LS3.

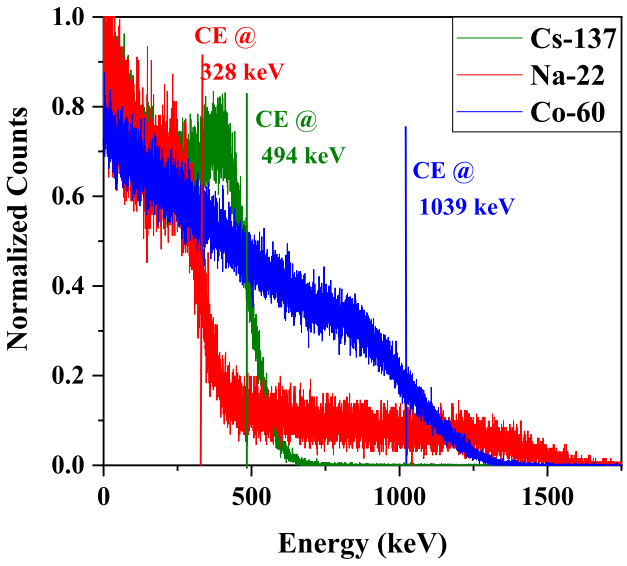

Fig. 9. Pulse height distribution of Cs-137, Na-22, and Co-60 demonstrating the Compton distribution as well as the location of the CE using LS1.

number of the ingredients in the LS. Generally, the GEANT4 simulation appears to have sharper CEs compared to the experimental results because GEANT4 assume ideal conditions and makes close to reality boundary conditions in the simulation. The simulation and experiment have difference in the concentration of dye. Simulation did not include the noise of the electrical signals created inside the PMT and other sources, such as the data acquisition electronics. The simulation may not accurately reflect the unique material characteristics and composition of the liquid scintillator employed in the experimental setup. For instance, the simulation model's assumptions about the atomic composition, density, concentration, and contaminants of the real liquid scintillator may not be accurate. The ideal geometry assumed to be a perfect cylinder, but experimental model has a contoured on the top also the glass thickness is accounted in simulation. These variances may affect how energy is deposited and how signals are generated afterwards, resulting in variations in the observed response. The primary objective of the simulation is to compare the CE and the agree with each other with a minimal error. It would take an incalculable amount of computational resource to exactly reproduce the experimental results as such in simulation (Mauritzson et al., n.d.; Sosa et al., n.d.).

Finally, the limitations were as follows, light yield and detection efficiency could be influenced by the concentration of Coumarin 450 and the dimensions of the scintillator used in the experimental setup, with potential variations not fully explored in this study. GEANT4 simulations, based on idealized conditions such as perfect geometry and

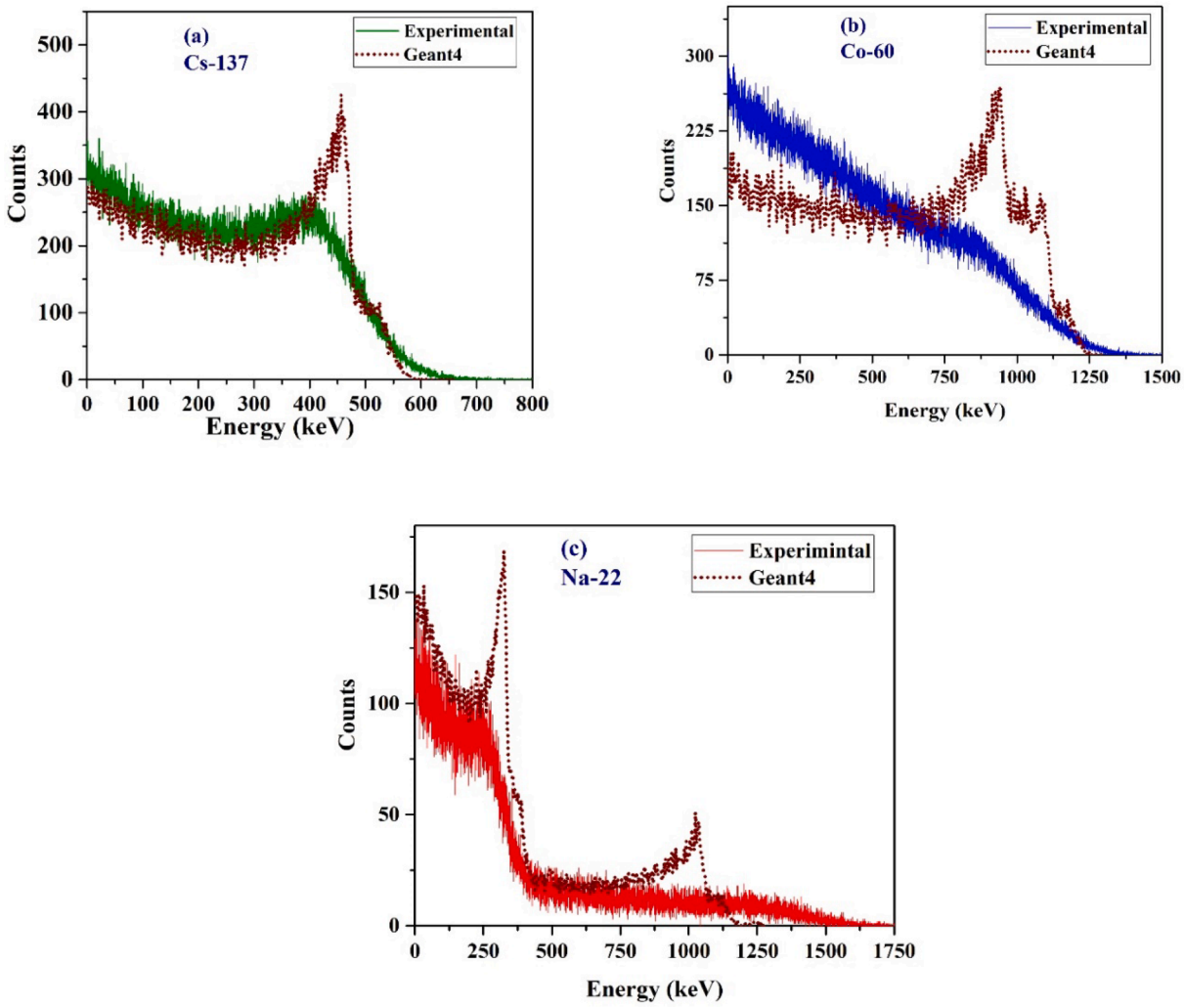

Fig. 10. Pulse height spectra for (a) Cs-137, (b) Co-60, and (c) Na-22 gamma sources using LS1 in comparison to the GEANT4 simulation results.

uniform material properties, may not accurately reflect real-world variations, leading to potential discrepancies between simulated and experimental results.

4. Conclusion

In this study, a simple liquid scintillator (LS) based on C450 dye was developed. The LS's light emission and counting efficiency (CE) could be adjusted by varying the concentration of the C450 dye. Three radioactive sources (Cs-137, Na-22, and Co-60) were used to evaluate the CE at different energy ranges. The optimal voltage for operations was determined to be −965 V. Experimental spectra of LS-1, LS-2, and LS-3 did not exhibit a clear CE edge. However, through Gaussian fitting of the shoulder and tail regions, the CE values were determined for each LS. For the Cs-137 source, LS-1 had a CE of 328 keV, LS-2 had a CE of 2995 Ch, and LS-3 had a CE of 2755 Ch. LS-1′s CE was 3.5 % lower than the theoretical value. LS-2 achieved a CE of 494 keV for the Na-22 source, exceeding the theoretical value by 3.4 %. The Co-60 gamma source produced two energies in the spectrum, with CEs of 963.39 and 1118.11 keV, resulting in an average CE of 1040.75 keV. The experimental CE of Co-60 closely matched the theoretical value, with an error of only 0.12 %. To validate the experimental results, a GEANT4 simulation of the LS was conducted. The theoretical calculations, experimental results (obtained through fitting), and simulation outcomes were found to be highly consistent. These LSs offer numerous benefits, including affordability, ease of mass production, and simple operation. They have minimal ingredient requirements and can be disposed of in an eco-friendly manner. Consequently, the LSs presented in this study hold great potential for the development of radiation detectors in various fields, such as medicine, military, and everyday life.

CRediT authorship contribution statement

Saradh Prasad: Supervision, Writing – review & editing, Writing – original draft, Investigation, Methodology, Conceptualization. **Nassar N. Asemi:** Writing – review & editing, Writing – original draft, Investigation, Conceptualization, Methodology. **Saad Aldawood:** Funding acquisition, Project administration, Supervision, Writing – review & editing, Resources, Methodology, Conceptualization. **Mohamad S. AlSalhi:** Funding acquisition, Project administration, Supervision, Writing – review & editing, Resources, Investigation, Methodology, Conceptualization.

Declaration of competing interest

The authors declare that they have no known competing financial interests or personal relationships that could have appeared to influence the work reported in this paper.

Acknowledgements

The authors extend their appreciation to the Deanship of Scientific

Research, King Saud University for funding through Vice Deanship of Scientific Research Chairs; Research Chair of Laser Diagnosis of Cancers.

Sample availability: available up on request

Samples of the fabricated scintillator are available from the corresponding author.

Appendix A. Supplementary data

Supplementary data to this article can be found online at https://doi.org/10.1016/j.jksus.2024.103160.

References

Aldawood, S., Asemi, N., Prasad, S., … M.A.-R.P. and, 2023, undefined, n.d. Design of DAMC dye as a liquid scintillator for gamma ray detection. Elsevier.

Arora, H., Aggarwal, A., Singh, R., 1982. Acid dissociation constants of electronically excited coumarins.

Asemi, N.N., Aljaafreh, M.J., Prasad, S., Aldawood, S., AlSalhi, M.S., Aldaghri, O., 2022. Efficient liquid scintillator loaded with a light-emitting conjugated oligomer for beta- and gamma-ray spectroscopic measurements. Radiat. Meas. 156, 106826 https://doi.org/10.1016/J.RADMEAS.2022.106826.

Brites, M., Santos, C., Nascimento, S., … B.G.-N. journal of, 2006, undefined, n.d. Synthesis and fluorescence properties of fullerene–coumarin dyads: Efficient dipole–dipole resonance energy transfer from coumarin to fullerene. pubs.rsc.org.

Chikkur, G.C., Umakantha, N., 1973. A new method of determining the Compton edge in liquid scintillators. Nucl. Instruments Methods 107, 201–202. https://doi.org/10.1016/0029-554X(73)90034-7.

Das, S.K., Sarkar, M., 2012. Steady-state and time-resolved fluorescence behavior of coumarin-153 in a hydrophobic ionic liquid and ionic liquid–toluene mixture. J. Mol. Liq. 165, 38–43.

Dhenadhayalan, N., Veeranepolian Selvi, A.S., Chellappan, S., Thiagarajan, V., 2021. Synergistic dynamics of photoionization and photoinduced electron transfer probed by laser flash photolysis and ultrafast fluorescence spectroscopy. Photochem. Photobiol. Sci. 20, 1109–1124. https://doi.org/10.1007/S43630-021-00084-0.

Gul, K., Naqvi, A., 1989. H.A.-J.M. in P.R.S., undefined, n.d. relative neutron detector efficiency and response function measurements with a 252Cf neutron source. Elsevier.

Gupta, M., Maity, D., Singh, M., 2012. S.N.-T.J. of, undefined, 2012. supramolecular interaction of coumarin 1 dye with cucurbit uril as host: combined experimental and theoretical study. ACS Publ. 116, 5551–5558. https://doi.org/10.1021/jp301266q.

Hajagos, T.J., Kishpaugh, D., Pei, Q., 2016. Pulse shape discrimination properties of plastic scintillators incorporating a rationally designed highly soluble and polymerizable derivative of 9,10-diphenylanthracene. nucl. instruments methods phys. res. sect. a accel. spectrometers. Detect. Assoc. Equip. 825, 40–50. https://doi.org/10.1016/J.NIMA.2016.04.029.

Ibnaouf, K.H., Prasad, S., Aldwayyan, A.S., Alsalhi, M.S., Masilamani, V., 2012. Amplified spontaneous emission spectra from the superexciplex of coumarin 138. Elsevier 97, 1145–1151. https://doi.org/10.1016/j.saa.2012.07.131.

Inagaki, S., Ohtani, O., Goto, Y., Okamoto, K., Ikai, M., Yamanaka, K.I., Tani, T., Okada, T., 2009. Light harvesting by a periodic mesoporous organosilica chromophore. Angew. Chemie Int. Ed. 48, 4042–4046. https://doi.org/10.1002/ANIE.200900266.

Jones, G., Jackson, W.R., Choi, C.Y., Bergmark, W.R., 1985. Solvent effects on emission yield and lifetime for coumarin laser dyes. requirements for a rotatory decay mechanism. J. Phys. Chem. 89, 294–300. https://doi.org/10.1021/J100248A024/SUPPL_FILE/J100248A024_SI_001.PDF.

Knoll, G.F., 2010. Radiation detection and measurement. John Wiley & Sons.

Knox, H., 1972. T.-M.-N.-I. Methods and, undefined. A technique for determining bias settings for organic scintillators. Elsevier, n.d.

Li, M., Guo, Z., Yeh, M., Wang, Z., Chen, S., 2016. Separation of scintillation and cherenkov lights in linear alkyl benzene. nucl. instruments methods phys. res. sect. a accel. spectrometers. Detect. Assoc. Equip. 830, 303–308. https://doi.org/10.1016/J.NIMA.2016.05.132.

Mahadevan, K., Masagalli, J., … H.H.-T.O., 2014, undefined, n.d. Synthesis and fluorescence study of some new blue light emitting 3-(1, 3-benzothiazol/benzoxazol-2-yl)-2H-chromen-2-ones. researchgate.net.

Mannekutla, J., Mulimani, B., A, s.i.-s.a.p.,, 2008. undefined, n.d. solvent effect on absorption and fluorescence spectra of coumarin laser dyes: evaluation of ground and excited state dipole moments. Elsevier.

Matta, A., Bahadur, V., Taniike, T., Van der Eycken, J., Singh, B.K., 2017. Synthesis, characterisation and photophysical studies of oxadiazolyl coumarin: a new class of blue light emitting fluorescent dyes. Dye. Pigment. 140, 250–260. https://doi.org/10.1016/J.DYEPIG.2017.01.050.

Mauritzson, N., Fissum, K., … H.P.-N.I. and, 2022, undefined, n.d. GEANT4-based calibration of an organic liquid scintillator. Elsevier.

Mir, F.A., Rather, S.A., Wani, I.A., Banday, J.A., Khan, S.H., 2014. Optical properties of some modified plant compound after 662 keV gamma radiation. Radiat. Eff. Defects Solids 169, 906–912. https://doi.org/10.1080/10420150.2014.961457.

Mir, F.A., Rehman, S.U., Khan, S.H., 2016. Gamma radiation response of plant isolated coumarin glycoside. Optik (stuttg). 127, 8361–8366. https://doi.org/10.1016/J.IJLEO.2016.06.039.

Mohan, D., Sharma, M., Singh, R., Pigments, V.S.-D. and, 2008, undefined, n.d. Estimation of molecular parameters in laser grade dyes: Coumarin 450 and Coumarin 460. Elsevier.

Naqvi, A.A., Al-Juwair, H., Gul, K., 1991. Energy resolution tests of 125 mm diameter cylindrical NE213 detector using monoenergetic gamma rays. Nucl. Instruments Methods Phys. Res. Sect. A 306 (1/2), 267–271. https://doi.org/10.1016/0168-9002(91)90331-J.

PARK, J., KIM, SB, LEE, J., KIM, B., KIM, SH, JOO, K., 2009. Feasibility study of a liquid scintillator using domestically produced Linear Alkyl Benzene (LAB).

Pla-Dalmau, A., Foster, G.W., Zhang, G., 1996. Gamma-irradiation of coumarins in a polystyrene matrix. Radiat. Phys. Chem. 48, 519–524. https://doi.org/10.1016/0969-806X(95)00474-C.

Porel, M., Klimczak, A., Freitag, M., Galoppini, E., Ramamurthy, V., 2012. Photoinduced electron transfer across a molecular wall: coumarin dyes as donors and methyl viologen and TiO 2 as acceptors. Langmuir 28, 3355–3359. https://doi.org/10.1021/LA300053R.

Prasad, S., Aljaafreh, M.J., Masilamani, V., AlSalhi, M.S., Mujamammi, W.M., 2020. Time-resolved excited state dynamics of super-exciplex in the coumarin dye laser. J. Mol. Liq. 315 https://doi.org/10.1016/J.MOLLIQ.2020.113814.

Prasad, S., Alsalhi, M.S., Kumar, R.S., Almansour, A.I., Arumugam, N., Alkaltham, M.F., Al-Shemaimari, K.I., Al-Tamimi, H., Bint, A., 2022. Synthesis, TD-DFT, and optical properties study of a chromeno-quinoline (acceptor) and mirror-less laser action enabled by energy transfer from a conjugated-polymer (donor). J. King Saud Univ. - Sci. 34 https://doi.org/10.1016/J.JKSUS.2022.102260.

Ravi, M., Soujanya, T., … A.S.-J. of the C., 1995, undefined, n.d. Excited-state dipole moments of some Coumarin dyes from a solvatochromic method using the solvent polarity parameter, ENT. pubs.rsc.org.

P. Saxena P.-R.-J. Technology of I.S. and 2018, undefined, Investigation on Optical Bistability and Excited State Absorption in Laser Grade Coumarin Dye. pubs.iscience. in 6 2018 19 24.

Sosa, C., Thompson, S., … D.C.-N.I. and, 2018, undefined, n.d. Energy resolution experiments of conical organic scintillators and a comparison with Geant4 simulations. Elsevier.

Tsoulfanidis, N., Landsberger, S., 2021. Measurement \& detection of radiation. CRC Press.

Zaitseva, N., Glenn, A., Mabe, A., 2018. M.C.-N.I. and, undefined. Recent developments in plastic scintillators with pulse shape discrimination. Elsevier, n.d.

Zaitseva, N.P., Glenn, A.M., Carman, M.L., Mabe, A.N., Payne, S.A., Marom, N., Wang, X., 2020. Multiple dye interactions in plastic scintillators: effects on pulse shape discrimination. Nucl. Instruments Methods Phys. Res. Sect. A Accel. Spectrometers, Detect. Assoc. Equip. 978 https://doi.org/10.1016/J.NIMA.2020.164455.

Zhang, X., Li, Z., 2013. Synthesis and fluorescence behavior of 2,5-diphenyl-1,3,4-oxadiazole-containing bismaleimides and bissuccinimides. Front. Chem. Sci. Eng. 2013 74 7, 381–387. https://doi.org/10.1007/S11705-013-1359-9.

Zhao, H., Yu, H., Redding, C., Li, Z., Chen, T., Meng, Y., Hajagos, T.J., Hayward, J.P., Pei, Q., 2021. Scintillation liquids loaded with hafnium oxide nanoparticles for spectral resolution of γrays. ACS Appl. Nano Mater. 4, 1220–1227. https://doi.org/10.1021/ACSANM.0C02845/SUPPL_FILE/AN0C02845_SI_001.PDF.